Journal of Non-Crystalline Solids 665 (2025) 123605

Contents lists available at ScienceDirect

Journal of Non-Crystalline Solids

journal homepage: www.elsevier.com/locate/jnoncrysol

Mechanism of void formation in high-density supercooled melts and amorphous alloys at negative external pressure

Bulat N. Galimzyanov *, Anatolii V. Mokshin

Kazan Federal University, 420008 Kazan, Russia
Udmurt Federal Research Center of the Ural Branch of RAS, 426067 Izhevsk, Russia

ARTICLE INFO

Keywords:
Void nucleation
Supercooled melts
Amorphous solids
Metal alloys
Thermodynamics
Molecular dynamics

ABSTRACT

Thermodynamic aspects of the void formation process are considered in detail on the basis of molecular dynamics simulation results. As an example, the comprehensive stretching of $Cu_{64.5}Zr_{35.5}$ and $Ni_{62}Nb_{38}$ at different supercooling levels is considered. Comprehensive stretching was performed by applying a constant negative external pressure. Within the framework of classical nucleation theory, new expressions have been obtained which correctly reproduce the critical size of voids and the Gibbs free energy as functions of supercooling. For the first time it was found that the critical size of the voids takes extremely small values — it is comparable to the size of the point defects, and the waiting time for the appearance of these voids does not exceed hundred picoseconds. General regularities of void formation have been revealed, suggesting the possibility of developing a unified theoretical description of void formation processes in supercooled melts and amorphous solids.

1. Introduction

The end of the 19th century can be considered as the beginning of a new era in the study of the nature of the void formation processes in materials. The active development of the transport industry, especially marine transport are significantly increased the interest in studying the mechanisms of bubble formation, growth and dissolution in liquids [1–4]. Essentially, research at the time was aimed to solving the problem of cavitation in ship propellers: the formation of bubbles around the rotating propeller leads to significant power loss and rapid blade wear. Lord Rayleigh's pioneering work [5] in the early 20th century about the collapse of spherical bubbles is clarified the understanding of the erosive effects of collapsing bubbles on propellers (see Fig. 1). The development of technologies for the refining petroleum products, manufacturing polymers, rubber and metal alloys for the construction of civil and military transport in the 30–40s of the 20th century are caused a rapid increase in theoretical and experimental works devoted to synthesis of soft and solid materials with porous structure [6–8]. During these years, the main attention was paid to the study of the fundamental problems of void formation in soft materials (rubber, gel, foam, etc.) as well as to the study of the mechanisms of nucleation and propagation of cracks in metal alloys.

The development of high-precision experimental techniques and their computerization in the 1980s and 1990s contribute to significant progress in understanding the initial stages of void formation, where the linear size of the voids is only a few nanometers [13–15]. The results of these studies provide the basis for various methods of foaming metal melts, including powder metallurgy methods. In the early 21st century, these methods were used to produce the first metal foams with both crystalline and amorphous matrices [19].

The research of the last decades is relevant for the development of experimental methods to control the crack formation process in solid materials [16,17,20,21]. For example, by Fokin et al. [16] it was found that phase transitions associated with crystallization can promote homogeneous void formation in supercooled melts. The reason for the appearance of such voids is the density mismatch between the initial amorphous phase and the forming crystallite, which leads to elastic stresses and disruption of the sequence of different crystalline phases occurrence. The results obtained by Mauro et al. [17] have been shown that crack formation and crack propagation in metal alloys can be controlled by nanoindentation: by indenting an object with rounded wedges into material. In addition, experimental and simulation results were obtained by Richard et al. [18] as well as Galimzyanov and Mokshin [22], where it was shown that the fracture of amorphous metal alloys under uniaxial and comprehensive stress is initiated by nucleation of nano-sized cracks. Theoretical studies performed by Kukushkin et al. [23,24] have provided phenomenological models to describe the evolution of micro-sized voids in materials under external stress. These

* Corresponding author at: Kazan Federal University, 420008 Kazan, Russia.
E-mail addresses: bulatgnmail@gmail.com (B.N. Galimzyanov), anatolii.mokshin@mail.ru (A.V. Mokshin).

https://doi.org/10.1016/j.jnoncrysol.2025.123605
Received 11 February 2025; Received in revised form 6 April 2025; Accepted 5 May 2025
Available online 22 May 2025

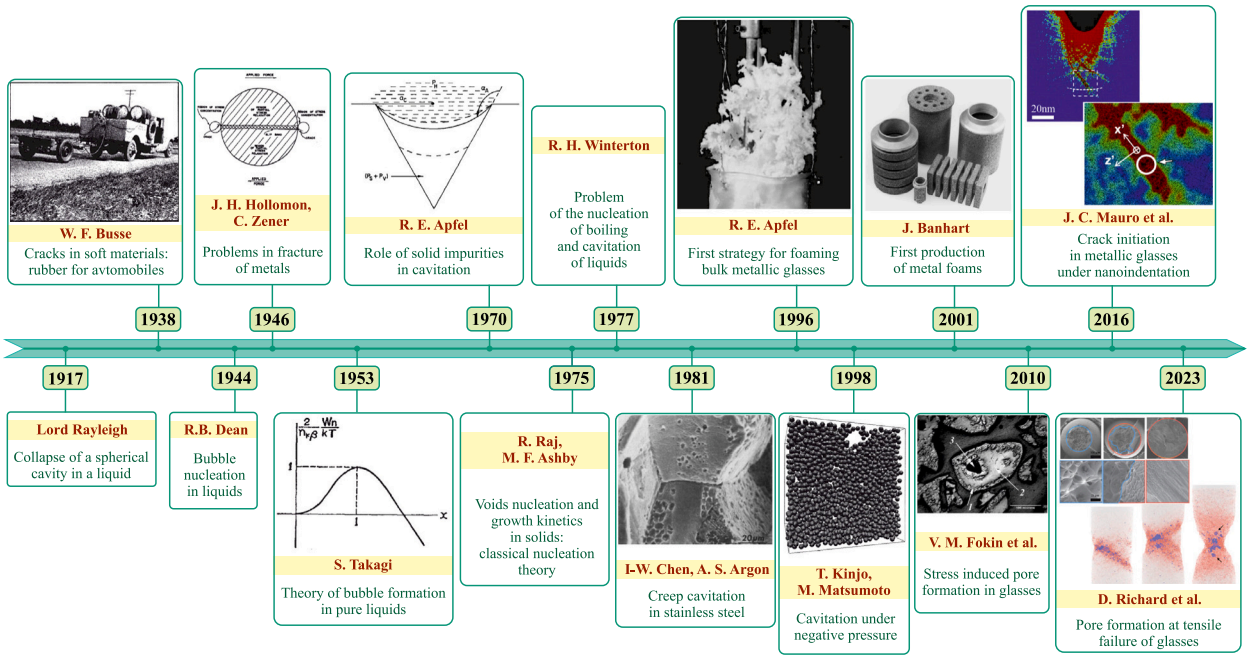

Fig. 1. Major milestones in the study of cavitation in soft and solid materials. This scheme is based on information taken from [5–19].

results reveal that the process of void growth in solids has much in common with the dendritic crystallization in supercooled metal melts.

Despite the achieved progress, very little attention has been paid to study the initial stages of void formation in supercooled melts and amorphous solids. The results of recent studies indicate that the void formation in such systems can occur under different scenarios. First, molecular dynamics simulation results of Falk et al. [25,26] reveal that the void nucleation in the amorphous $Zr_{50}Cu_{50}$ alloy can follow a heterogeneous scenario. As found, nucleation always occurs at the same location in the sample, where there is a high structural susceptibility to plastic deformation. On the other hand, void formation in supercooled melts and amorphous solids can follow a homogeneous scenario without favored regions, when a system does not contain crystalline inclusions that can act as seeds for structural transformations [27–31]. Therefore, the aim of the present work is the quantitative characterization and theoretical description of the initial stages of void nucleation on the example of $Cu_{64.5}Zr_{35.5}$ and $Ni_{62}Nb_{38}$ alloys during comprehensive stretching initiated by external negative pressure [32–34]. The applicability of the classical nucleation theory to describe the thermodynamic characteristics of the void nucleation in these systems is verified.

2. Void nucleation in solids: theoretical aspects

From point of view of thermodynamics, the process of void formation in solids has much in common with the processes of crystallization and condensation [35–37]. In all these processes, a system may be far from thermodynamic equilibrium either due to supercooling or due to the action of a constant external mechanical stress. Ray and Ashby were probably the first to point out that the concept of classical nucleation theory can be applied to describe the process of void formation in solids [11,38]. According to this, the general expression for determining the Gibbs free energy $\Delta G(r)$ required for the formation of a void with the curvature radius r can be expressed in the following form [11]:

$$\Delta G(r) = -C_v(\theta) r^3 \sigma(p, T) + C_s(\theta) r^2 \gamma(p, T) - C_b(\theta) r^2 \gamma_b(p, T). \quad (1)$$

Here, the contribution $C_v(\theta) r^3 \sigma(p, T)$ determines the free energy required to form a void; the contribution $C_s(\theta) r^2 \gamma(p, T)$ is the surface free energy of a void; the contribution $C_b(\theta) r^2 \gamma_b(p, T)$ defines the surface free energy of the void walls, where p and T are the pressure and temperature, respectively. In Eq. (1), the quantity $\gamma(p, T)$ is the interfacial tension between a solid phase and a void, while $\gamma_b(p, T)$ defines the interfacial tension of a solid phase. The quantities $\gamma(p, T)$ and $\gamma_b(p, T)$ are related by the Young-Dupre equation [39,40]:

$$\frac{\gamma_b(p, T)}{\gamma(p, T)} = 2\cos\theta, \quad (2)$$

where θ is the angle between the tangent plane and the normal to the void surface [see Fig. 2(a)]. The dimensionless coefficients C_v, C_s and C_b characterize a shape of the void and are defined as follows:

$$C_v(\theta) = \frac{2\pi}{3}(2 - 3\cos\theta + \cos^3\theta), \quad (3)$$

$$C_s(\theta) = 4\pi(1 - \cos\theta), \quad (4)$$

$$C_b(\theta) = \pi \sin^2\theta. \quad (5)$$

In the case of a spherical void, the radius of curvature r coincides with the radius of the void at all points on the surface, as shown in Fig. 2(b). Here we have the angle $\theta = 90°$ and Eqs. (2), (3)–(5) take the following forms:

$$\gamma_b(p, T) = 0, \quad C_v(\theta = 90°) = \frac{4\pi}{3}, \quad C_s(\theta = 90°) = 4\pi, \quad C_b(\theta = 90°) = \pi. \quad (6)$$

Then it follows from (1) and (6) that the Gibbs free energy $\Delta G(r)$ for the formation of a void with spherical shape and of the radius r under the comprehensive tensile stress is determined as

$$\Delta G(r) = -\frac{4\pi}{3} r^3 \sigma(p, T) + 4\pi r^2 \gamma(p, T). \quad (7)$$

According [11], the quantity $\sigma(p, T)$ in Eq. (7) is the tensile stress. This tensile stress is the driving force of the void nucleation process at pressure p and temperature T [40,41]. Here, the quantity $\sigma(p, T)$ is similar to the difference in chemical potentials $|\Delta\mu(p, T)|$ between the initial parent phase and the forming daughter phase for crystal nucleation or condensation processes [35–37]. The quantity $\sigma(p, T)$ is directly determined by the diagonal components of the stress tensor $\sigma_{\alpha\alpha}(p, T)$, where $\alpha = \{x, y, z\}$, i.e. $\sigma(p, T) \equiv \sigma_{\alpha\alpha}(p, T)$, which are equal

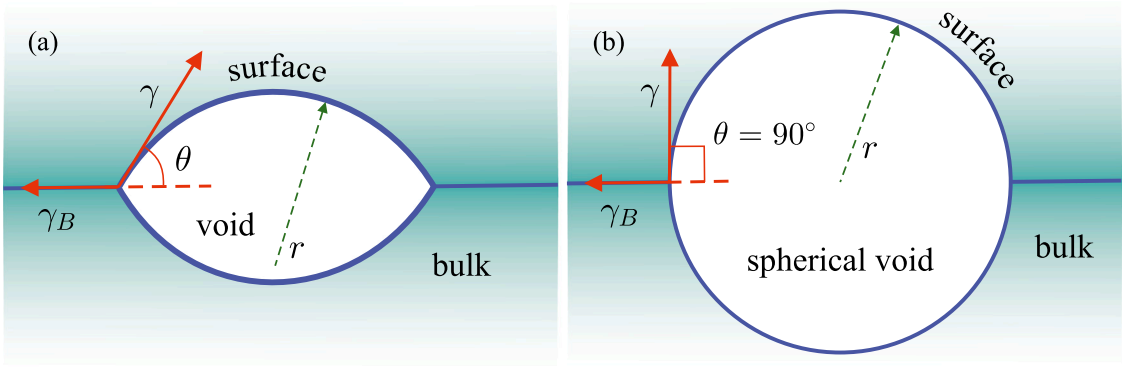

Fig. 2. (a) Schematic representation of a lenticular void with the curvature radius r. (b) View of a spherical void whose radius coincides with the curvature radius r.

to each other when a system is stretched in all directions: $\sigma_{xx}(p, T) = \sigma_{yy}(p, T) = \sigma_{zz}(p, T)$. In the present work, we consider the mechanical stress as the average of the diagonal components, i.e. $\sigma(p,T) = [\sigma_{xx}(p,T) + \sigma_{yy}(p,T) + \sigma_{zz}(p,T)]/3$. The quantitative characterization of $\sigma_{\alpha\alpha}(p, T)$ can be performed by the Irwin-Kirkwood method based on the results of molecular dynamics simulations [42,43]:

$$\sigma_{\alpha\alpha}(p, T) = -\frac{1}{V(p, T)}\left(\sum_{i=1}^{N} m_i[v_{i\alpha}(p, T)]^2 + \sum_{i=1}^{N}\sum_{j>i}^{N} r_{ij\alpha}F_{ij\alpha}\right). \quad (8)$$

Here, $v_{i\alpha}(p, T)$ is the α-component of the velocity of the ith atom with the mass m_i; $r_{ij\alpha}$ and $F_{ij\alpha}$ are the distance and the interaction force between atoms of index i and j in projection on the α-axis; $V(p, T)$ is the volume of a system; N is the number of all atoms in a system.

In Eq. (7), it is assumed that void formation is an activation-type process: when the average void radius reaches the critical radius r_c, a void becomes capable of further growth. The formation of such a void occurs with some waiting time τ_c necessary for the formation of a critically sized void after the system is removed from the thermodynamic equilibrium state. In this case, the values of the free energy $\Delta G(r)$ become maximal at $r = r_c$, which can be taken into account by the following condition:

$$\left.\frac{\partial \Delta G(r)}{\partial r}\right|_{r=r_c} = 0. \quad (9)$$

From Eqs. (7) and (9) we obtain the following equation:

$$-4\pi r_c^2\sigma_c(p, T) + 8\pi r_c\gamma_c(p, T) = 0. \quad (10)$$

Here, the quantity $\sigma_c(p, T)$ characterizes the ultimate tensile strength of the system at which a void of the critical radius r_c with the surface tension $\gamma_c(p, T)$ is formed. The critical radius r_c is determined from Eq. (10) as

$$r_c = \frac{2\gamma_c(p, T)}{\sigma_c(p, T)}, \quad (11)$$

whereas the free energy ΔG_{r_c} of a void with the critical radius r_c is determined by the equation

$$\Delta G_{r_c} = \frac{16\pi}{3}\frac{[\gamma_c(p, T)]^3}{[\sigma_c(p, T)]^2}. \quad (12)$$

As known by now, such the characteristics of critical grains of a new formed phase as the critical size and the appearance (or waiting) time are correctly determined by the statistical method developed on the basis of the mean first-passage time approach [44,45]. According to this method, a set of trajectories characterizing the sizes of the largest voids in the systems at successive time points from independent experiments is analyzed. For each trajectory, a set of times of the first appearance of a void of a certain radius is determined, and the distribution $\tau(r)$ for each experiment is evaluated. The obtained distributions $\tau(r)$ are averaged and the most probable void appearance times of different radii are determined. In this approach, it is not necessary that a separately considered trajectory characterizes the evolution of a single grain of the new phase (in our case, this is a void). Next, the critical radius r_c and the average waiting time τ_c are determined from the analysis of the resulting distributions $\bar{\tau}(r)$, and the first derivative of this distribution, $\partial\bar{\tau}(r)/\partial r$. The point of extremum (maximum) in the derivative $\partial\bar{\tau}(r)/\partial r$ corresponding to the location of the inflection point in the distribution $\bar{\tau}(r)$, determines the critical radius r_c, while the time $\tau(r = r_c) \equiv \tau_c$ is directly related to the average waiting time for a critically sized void to appear.

3. Void nucleation in supercooled $Cu_{64.5}Zr_{35.5}$ and $Ni_{62}Nb_{38}$ melts

Molecular dynamics simulations of void nucleation under comprehensive stretching have been performed on the example of $Cu_{64.5}Zr_{35.5}$ and $Ni_{62}Nb_{38}$ systems. Each system consists of 31 250 atoms: 20 156 Cu atoms and 11 094 Zr atoms in the case of $Cu_{64.5}Zr_{35.5}$; 19 375 Ni atoms and 11 875 Nb atoms for $Ni_{62}Nb_{38}$. This number of atoms is sufficient to minimize finite size effects when simulating the formation of nanoscale voids in these systems. The interaction between the atoms is given by the EAM type potential with Mendelev's parameterization [46,47]. As found before [46,47], the potential correctly reproduces the atomic dynamics and structure of these systems in liquid and amorphous states. The integration of the equations of motion for all atoms is performed with the time step 2 fs. First, we consider the samples with different supercooling T/T_l: at $T/T_l = 0.24$ (in the case of $Cu_{64.5}Zr_{35.5}$) and $T/T_l = 0.19$ (in the case of $Ni_{62}Nb_{38}$) corresponding to the room temperature $T = 300$ K. The systems with the supercooling $T/T_l = 0.48$, 0.72 and 0.96 are also considered. According to the known phase diagrams of these systems [48,49], the liquidus temperature of $Cu_{64.5}Zr_{35.5}$ is $T_l = 1250$ K and $T_l = 1550$ K for $Ni_{62}Nb_{38}$ on the isobar $p = 1$ atm. The external negative pressure is realized in the NpT ensemble is realized by the Nose–Hoover thermostat and barostat with the parameters 0.25 ps and 2 ps, respectively. We have used the constant negative pressure $p = -12$ GPa, which allows us to simulate the comprehensive stretching under which the considered systems would be in a metastable state. This pressure was chosen so that the waiting time for void nucleation was less than the structural relaxation time of the system under external tensile stress. Thus, these considered (p, T)-conditions will favor the homogeneous void nucleation inside the systems on the time scales available for molecular dynamics simulations [see Figs. 3 and 4]. For the statistical treatment of the obtained results, ten independent simulations were performed for each system.

The process of structural change in $Cu_{64.5}Zr_{35.5}$ and $Ni_{62}Nb_{38}$ under stretching occurs in several stages. In the first stage, the stretching leads to a decrease in the average density of the samples and the formation of excess free volume. The density of $Cu_{64.5}Zr_{35.5}$ decreases from 7.5 g/cm^3 to 6.5 g/cm^3, while the density of $Ni_{62}Nb_{38}$ decreases from 8.8 g/cm^3 to 7.4 g/cm^3. The attractive forces between the atoms

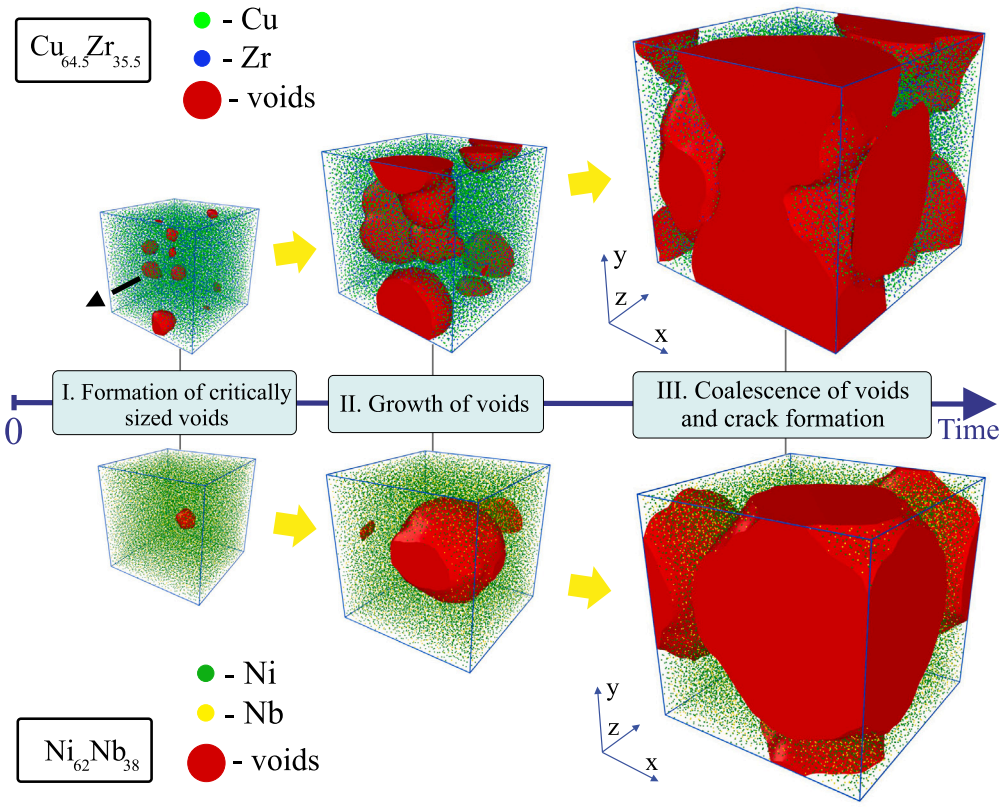

Fig. 3. Snapshots of supercooled $Cu_{64.5}Zr_{35.5}$ and $Ni_{62}Nb_{38}$ melts at different stages of void formation during comprehensive tensile stress: (I) formation of a critically sized void, (II) void growth and (III) void coalescence. These snapshots were obtained at the supercooling $T/T_l = 0.48$ that corresponds to the temperature $T = 600$ K.

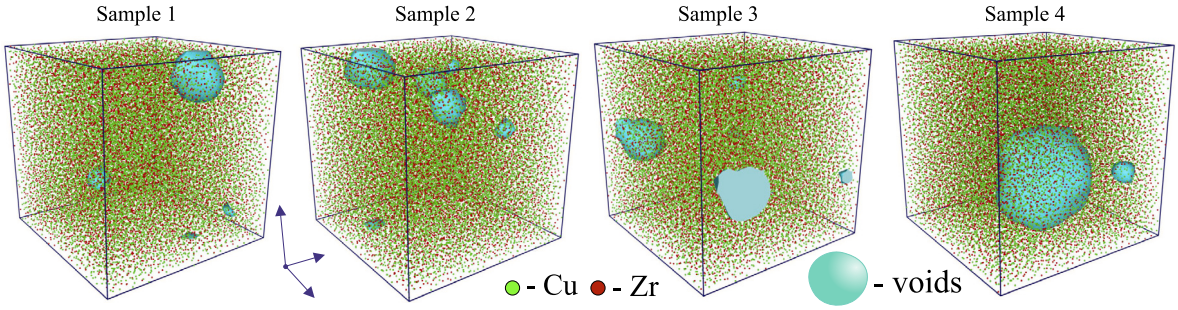

Fig. 4. Snapshots of four different samples for supercooled $Cu_{64.5}Zr_{35.5}$ melts, where the system contains the voids. Here, the supercooling is $T/T_l = 0.24$. The void formation process follows the homogeneous scenario.

prevent the interatomic bonds from breaking. As a result, both the systems exhibit elastic response, and the structure of these systems is restored without any visible defects when the external stress is removed. In the second stage, the interatomic bonds are broken and stable voids of relatively small size are formed due to the redistribution of local stresses. The third stage is associated with the stable growth of voids and their coalescence. For example, as shown in Fig. 3, the coalescence of voids leads to the formation of percolation tunnels/cracks. The visualization of these voids was performed using the method of Stukowski [50].

For the identification of voids, including critically sized voids, we used the method of filling voids with virtual particles [22]. According to this method, a three-dimensional grid is constructed, which divides the simulation cell into cubic segments with the same edge length $\sigma/2$, where σ is the effective average diameter of the real atoms in a system. In the case of the considered systems, the number of such segments is more than 150 000. A virtual particle with the diameter σ is placed in each segment of this grid. If this particle does not intersect with real atoms of the system and with other virtual particles, the position of this virtual particle in the selected segment is fixed. Otherwise, the virtual particle is removed. This procedure continues until all voids are filled with virtual particles. Furthermore, the number of virtual particles inside the voids is determined at each time point of the simulation. Each virtual particle is characterized by a coordinate and a unique identification number, which allows us to determine the growth trajectory of each individual void in the system (i.e., the dependence of the void size on time). Here, the size refers to the volume of a void, which is calculated as the sum of the volumes of the virtual particles located in this void. Considering that the shape of voids at the stage of nucleation is close to spherical [as it is shown in Fig. 4], the linear size (i.e. radius) of a void is determined from its known volume.

The growth curves of the largest voids obtained at different supercooling levels and reduced by the critical radius r_c and the waiting time τ_c are similar [see Figs. 5(a) and 5(b)]. This suggests a common physical mechanism of void formation in supercooled $Cu_{64.5}Zr_{35.5}$ and $Ni_{62}Nb_{38}$ melts. The dependence of the reduced radius r/r_c on the reduced time

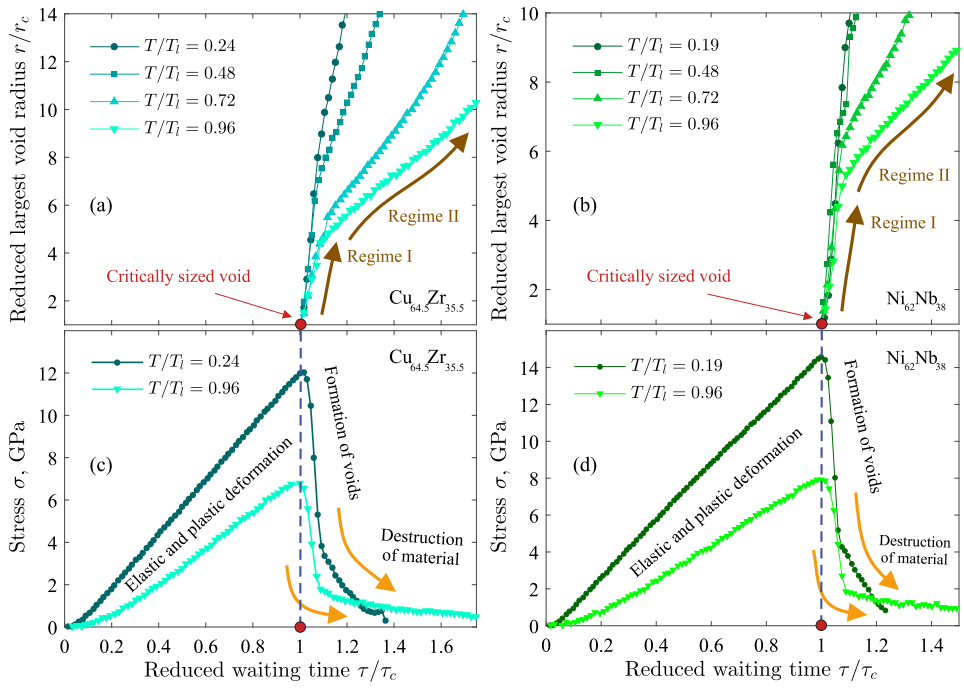

Fig. 5. Reduced radius r/r_c of the largest void as a function of the reduced waiting time τ/τ_c calculated at different supercooling T/T_l for the comprehensive tensile stress of supercooled (a) $Cu_{64.5}Zr_{35.5}$ and (b) $Ni_{62}Nb_{38}$ melts. The quantity r_c is the critical radius of the void, whereas τ_c is the nucleation waiting time for the critically sized void. Stress σ as a function of the quantity τ/τ_c calculated by Eq. (8): (c) for $Cu_{64.5}Zr_{35.5}$ and (d) for $Ni_{62}Nb_{38}$. Here $\sigma = (\sigma_{xx} + \sigma_{yy} + \sigma_{zz})/3$. Yellow arrows show the inflections that occur due to the formation of nano-sized cracks.

τ/τ_c has two regimes, which become pronounced as the supercooling of the systems decreases. The first regime is associated with void surface formation, while the second regime is associated with void coalescence. Figs. 5(c) and 5(d) show that the internal stress σ as a function of the reduced waiting time τ/τ_c has a linear regime, which is related to the elastic behavior of the systems. The maximum in the function $\sigma(\tau/\tau_c)$ corresponds to the ultimate tensile strength σ_c, at which the system starts to destroy. This maximum is reached exactly before the appearance of the first nucleation event associated with the formation of a viable void, and the formation of this void provokes the release of internal stress. It is, therefore, quite understandable that in the statistical treatment the most probable time of reaching the maximum stress practically coincides with the most probable appearance time of the first critically sized void. At the same time, as can be seen from the results (Fig. 5), the stress is not released instantaneously, but decreases according to a time-dependent law. The quantity σ_c depends on the supercooling: the higher the supercooling (i.e. the lower T/T_l), the higher the value of the tensile strength. In particular, for $Cu_{64.5}Zr_{35.5}$ the maximum stress decreases from $\sigma_c \simeq 11.9$ to 6.65 GPa with decreasing supercooling, while for $Ni_{62}Nb_{38}$ the decrease is from $\sigma_c \simeq 14.6$ to 7.93 GPa.

Note that the evaluation of void nucleation characteristics is carried out at the initial stage, when the volume of the formed voids is significantly smaller than the volume of the simulated systems. For example, at the stage of void nuletaion, the average volume of the $Ni_{62}Nb_{38}$ and $Cu_{64.5}Zr_{35.5}$ systems is $V \approx (3.7\pm0.4)\times10^5$ Å^3 and $V \approx (4.8\pm0.3)\times10^5$ Å^3, respectively, whereas the total volume of all voids (averaged over the considered supercooling range) is $V_p \approx (2400 \pm 300)$ Å^3 and $V_p \approx (8500 \pm 1000)$ Å^3 for these systems, correspondingly. Thus, the fraction of critically sized voids is only $V/V_p \approx 0.6\%$ of the total volume of the $Ni_{62}Nb_{38}$ system and $V/V_p \approx 1.8\%$ in the case of $Cu_{64.5}Zr_{35.5}$. Thus, the finite size effects should not appear at such the correspondence between the volumes V and V_p.

4. Thermodynamic aspects of the void nucleation

4.1. Surface tension of critically sized voids

The estimation of the surface tension $\gamma_c \equiv \gamma_c(p, T)$ of a void with the critical radius r_c is performed using Eq. (11). In this equation, values of the quantities r_c and σ_c are determined from molecular dynamics simulations [see Table 1]. Fig. 6(a) shows the resulting dependence of the surface tension γ_c on the supercooling T/T_l, which follows the empirical Eötvös rule [51]. According to this rule, the quantity γ_c as a function of temperature T follows a linear dependence and decreases with temperature:

$$\gamma_c(T/T_l) = \gamma_1 \left(\gamma_2 - \frac{T}{T_l}\right). \tag{13}$$

Here, the coefficients γ_1 and γ_2 take only positive values and depend on the material composition. In the case of $Cu_{64.5}Zr_{35.5}$, we have $\gamma_1 \simeq 0.0194$ eV/Å^2 and $\gamma_2 \simeq 5.5$, while for $Ni_{62}Nb_{38}$ the coefficient values are $\gamma_1 \simeq 0.0382$ eV/Å^2 and $\gamma_2 \simeq 3.25$. The coefficient $\gamma_1 \approx T_l k/V_m^{2/3}$ is the Eötvös constant, where V_m is the molar volume and $k = 2.1 \times 10^{-7}$ J/(K·mol$^{-2/3}$). The values of the coefficient γ_1 were determined on the basis of the known molar volumes of the chemical elements of the considered systems ($V_m \approx 21.1$ cm^3/mol for $Cu_{64.5}Zr_{35.5}$ and $V_m \approx 17.4$ cm^3/mol for $Ni_{62}Nb_{38}$) and the liquidus temperatures ($T_l \simeq 1250$ K for $Cu_{64.5}Zr_{35.5}$ and $T_l \simeq 1550$ K for $Ni_{62}Nb_{38}$). The found value of the coefficient γ_2 corresponds to the reduced temperature T_c/T_l, at which the surface tension becomes zero. According to these results, the assumed critical temperature T_c for $Cu_{64.5}Zr_{35.5}$ is $T_c \approx 6880$ K, and for $Ni_{62}Nb_{38}$ we have $T_c \approx 5040$ K.

4.2. Ultimate tensile strength for critically sized voids

Currently, there are a wide variety of models for the temperature dependence of the ultimate tensile strength σ_c, including the empirical relationship proposed by Dureja et al. for metal alloys [52], the regression models proposed by Lee et al. and Wang et al. for steel [53,54], the

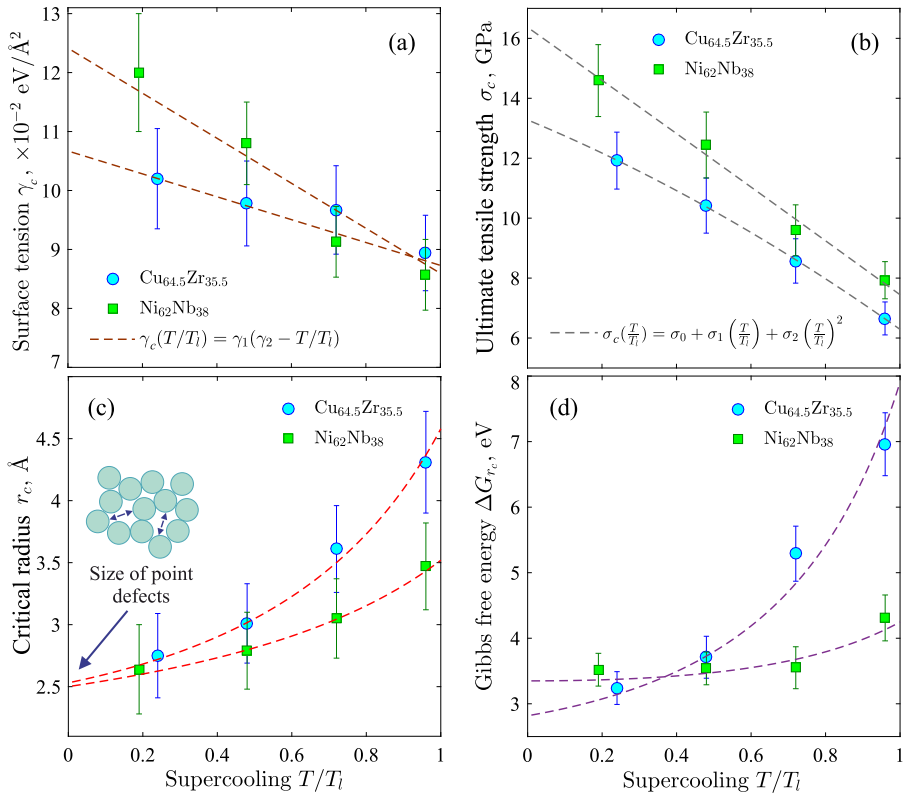

Fig. 6. Void nucleation characteristics as a function of supercooling T/T_l: (a) surface tension γ_c of the critically sized voids, (b) tensile strength σ_c of the system when the critically sized voids are formed, (c) critical radius r_c and (d) Gibbs free energy ΔG_{r_c} for the critically sized voids. These results were obtained by molecular dynamics simulations for supercooled $Cu_{64.5}Zr_{35.5}$ and $Ni_{62}Nb_{38}$ melts using Eqs. (8), (11) and (12). The dashed lines are the results of Eqs. (13), (15), (16) and (17).

piecewise fitting formula obtained by Ban et al. for metal alloys [55], the temperature-dependent model with piecewise fitting parameters suggested by Chen and Young [56] and the model based on the force-heat equivalence energy density principle proposed by He et al. for metallic materials [57]. In general, according to these models, the quantity σ_c can be represented as a function of the supercooling T/T_l in the polynomial form:

$$\sigma_c(T/T_l) = \sum_{i=0}^{n} \sigma_i \left(\frac{T}{T_l}\right)^i. \tag{14}$$

Here, the values of the parameters σ_0, σ_1, $\cdots$, σ_n and the exponent n depend on the composition of the system and are determined by fitting to the experimental data. As can be seen from Fig. 6(b), full agreement between the simulation results and Eq. (14) is achieved in the case of a second degree polynomial:

$$\sigma_c(T/T_l) = \sigma_0 + \sigma_1\left(\frac{T}{T_l}\right) + \sigma_2\left(\frac{T}{T_l}\right)^2. \tag{15}$$

Here, $\sigma_0 \simeq 13.3$ GPa, $\sigma_1 \simeq -5.18$ GPa, $\sigma_2 \simeq -1.814$ GPa for $Cu_{64.5}Zr_{35.5}$ and $\sigma_0 \simeq 16.4$ GPa, $\sigma_1 \simeq -8.83$ GPa, $\sigma_2 \simeq -0.0935$ GPa for $Ni_{62}Nb_{38}$. The found values of the parameters are comparable to those previously obtained for other metallic materials. For example, according to the model of Lee et al. the values of these parameters for steel are $\sigma_0 \sim 0.7$ GPa, $\sigma_1 \sim -2.37$ GPa, and $\sigma_2 \sim -9.5$ GPa [52,57].

4.3. Critical radius and activation energy as functions of supercooling

Using Eq. (13) for the surface tension γ_c and Eq. (15) for the tensile strength σ_c, we present Eqs. (11) and (12) in the following forms:

$$r_c(T/T_l) = \frac{2\gamma_1\left(\gamma_2 - \frac{T}{T_l}\right)}{\sum_{i=0}^{2}\sigma_i\left(\frac{T}{T_l}\right)^2}, \tag{16}$$

$$\Delta G_{r_c}(T/T_l) = \frac{16\pi}{3}\frac{\left[\gamma_1\left(\gamma_2 - \frac{T}{T_l}\right)\right]^3}{\left[\sum_{i=0}^{2}\sigma_i\left(\frac{T}{T_l}\right)^2\right]^2}. \tag{17}$$

Figs. 6(c) and 6(d) show that Eqs. (16) and (17) correctly reproduce the dependence of the critical radius r_c and the activation energy ΔG_{r_c} on the supercooling T/T_l. At extremely deep supercooling (i.e. at $T/T_l \to 0$), the critical radius tends to the size of the point defects [see Fig. 6(c)]. The activation energy is $\Delta G_{r_c} \sim 3$ eV, which is comparable to the energy for vacancy (crystal defect) formation in Ni- and Cu-based alloys [58]. On the other hand, an increase in the critical radius r_c and the activation energy ΔG_{r_c} is observed with decreasing supercooling. This is due to the fact that the system becomes less viscous with increasing temperature and such a system relieves internal stress. Thus, a large work $A = \Delta G_{r_c}$ is required to break the interatomic bonds and form a void with a relatively large critical radius [see Fig. 6(d)].

4.4. Comparison of $Cu_{64.5}$ $Zr_{35.5}$ and $Ni_{62}Nb_{38}$

Comparison of the results obtained for supercooled $Cu_{64.5}Zr_{35.5}$ and $Ni_{62}Nb_{38}$ melts shows that the appearance of the voids and local fracture zones in the samples follows a common homogeneous nucleation scenario. The thermodynamic characteristics of void nucleation are correctly described by Eqs. (13), (14), (16) and (17) obtained in the framework of the classical nucleation theory. The critical radius r_c and the activation energy ΔG_{r_c} are slightly larger in the case of $Cu_{64.5}Zr_{35.5}$ than in the case of $Ni_{62}Nb_{38}$ under thermodynamically identical conditions. Such a difference in the values of the nucleation characteristics is mainly due to the specificity of the interatomic interaction and the composition of these systems. Both the systems $Cu_{64.5}Zr_{35.5}$ and $Ni_{62}Nb_{38}$ are able to form a distorted icosahedral structure in the supercooled state [59–61]. The $Ni_{62}Nb_{38}$ system is less sensitive to the change in the

Table 1
Thermodynamic characteristics of the critically sized voids at the different supercooling T/T_l: temperature T; critical radius r_c; waiting time τ_c; tensile strength σ_c when critically sized voids are formed; Gibbs free energy ΔG_{r_c} and surface tension γ_c.

System	T/T_l	T, K	r_c, Å	τ_c, ps	σ_c, GPa	ΔG_{r_c}, eV	γ_c, $\times 10^{-2}$eV/Å^2
$Cu_{64.5}Zr_{35.5}$	0.24	300	2.75 ± 0.34	22.0 ± 2.3	11.92 ± 0.95	3.24 ± 0.25	10.2 ± 0.85
	0.48	600	3.01 ± 0.32	21.2 ± 2.4	10.42 ± 0.92	3.71 ± 0.32	9.78 ± 0.72
	0.72	900	3.61 ± 0.35	19.7 ± 2.1	8.572 ± 0.74	5.29 ± 0.42	9.67 ± 0.75
	0.96	1200	4.31 ± 0.41	18.7 ± 1.8	6.654 ± 0.55	6.96 ± 0.48	8.94 ± 0.64
$Ni_{62}Nb_{38}$	0.19	300	2.64 ± 0.36	26.7 ± 2.5	14.59 ± 1.2	3.52 ± 0.25	12.0 ± 1.0
	0.48	745	2.79 ± 0.31	25.9 ± 2.1	12.44 ± 1.1	3.54 ± 0.25	10.8 ± 0.7
	0.72	1115	3.05 ± 0.32	24.8 ± 2.3	9.594 ± 0.85	3.55 ± 0.32	9.13 ± 0.6
	0.96	1490	3.47 ± 0.35	22.3 ± 2.0	7.929 ± 0.62	4.31 ± 0.35	8.57 ± 0.6

fraction of distorted icosahedra with increasing supercooling compared to $Cu_{64.5}Zr_{35.5}$ [61]. The relatively high content of such icosahedra in $Cu_{64.5}Zr_{35.5}$ may lead to a decrease in the binding energy between interacting atoms due to the presence of interatomic voids [62]. This favors the formation of large voids and increases the free energy of void formation during the comprehensive stretching of the system, as observed from the obtained results.

5. Conclusions

In the present work, using the amorphous metallic systems $Ni_{62}Nb_{38}$ and $Cu_{64.5}Zr_{35.5}$, the thermodynamic characteristics of the process of homogeneous void nucleation have been determined for the first time in the wide supercooling range: the critical void radius r_c as well as the surface tension γ_c and the Gibbs free energy ΔG_{r_c} for critically sized voids. New expressions (16) and (17) for r_c and ΔG_{r_c} are obtained, which correctly reproduce the simulation results and give correct asymptotics in the limiting cases as $T \to 0$ and $T \to T_l$. Such results have not yet been reported in the scientific literature. The correctness of the obtained expressions is confirmed by the fact that they are based on known empirical rules and relationships (e.g. equations of the classical nucleation theory, empirical Eötvös rule, empirical relationship of Dureja et al. regression models proposed by Lee et al. and Wang et al.) for the temperature dependences of surface tension and tensile strength. In addition, it is shown in the present work that critically sized voids play an important role in the fracture of materials. The appearance of critical voids initiates crack formation and thus the process of material fracture. This conclusion is in good agreement with the results of previous studies on the fracture mechanisms of solids [25,63–65]. Thus, the obtained results can be extended to other types of materials and contribute significantly to the existing knowledge of the physics of material fracture processes.

It should be noted that, most of the experimental scientific works are aimed at consideration of macroscopic mechanisms of crack formation and very rarely touch upon the initial stages of nucleation of nanoscale voids. This is due to the difficulty of detecting their presence in the bulk of a material due to their extremely small size and extremely low concentration at the nucleation stage. Nevertheless, nucleation of voids in metal alloys has been studied in several experimental works [18,40,66,67]. For example, in the work of F. Meixner et al. [40], a model based on the classical nucleation theory and complemented with existing models of nucleus growth was proposed. This model has demonstrated its applicability to Ni-based alloys during creep tests and correctly determines the size and shape of voids and their growth trajectory. The empirical results obtained by D. Richard et al. [18], L.-Q. Shen et al. [66] and B. Sarac et al. [67] show that the fracture of amorphous materials under tensile strain can be initiated after the formation of nano-sized voids (or critical length cracks). The results of our study support and extend the conclusions presented in these works.

The study of the initial stages of the fracture process of materials and, in particular, amorphous metal alloys, is an important task both from a fundamental scientific point of view and from a practical one. So, at present there is no generally accepted theory describing the initial stages of fracture formation centers [9,15,16,25]. The development of classical nucleation theory, which was originally developed to describe the initial stages of the first-order phase transitions, seems promising. This is especially true for such isotropic systems as amorphous metal alloys. It is obvious that in crystalline materials the processes of formation of local fracture centers will be different due to the structural anisotropy of these materials. From a practical point of view, there is a need to develop the methods that would make it possible to control or prevent the formation of voids (cracks) in order to extend the service life of materials. The study of the mechanisms by which voids can "self-heal" is promising. The results of recent studies show that pure metals and their alloys can "heal" nano-sized pores under certain conditions [68–70]. This is important for the design of fatigue resistant materials.

CRediT authorship contribution statement

Bulat N. Galimzyanov: Writing – original draft, Methodology, Investigation, Formal analysis. **Anatolii V. Mokshin:** Writing – review & editing, Writing – original draft, Conceptualization.

Declaration of competing interest

The authors declare that they have no known competing financial interests or personal relationships that could have appeared to influence the work reported in this paper.

Acknowledgments

The work was carried out on the basis of the grant provided by the Academy of Sciences of the Republic of Tatarstan in 2024 for the implementation of fundamental and applied research work in scientific and educational organizations, enterprises and organizations of the real sector of the economy of the Republic of Tatarstan.

References

[1] C.E. Brennen, Cavitation and Bubble Dynamics, Oxford University Press, New York, Oxford, 1995.
[2] V.P. Skripov, Metastable Liquids, Wiley, New-York, 1974.
[3] D.E. Yount, E.W. Gillary, D.C. Hoffman, A microscopic investigation of bubble formation nuclei, J. Acoust. Soc. Am. 76 (1984) 1511–1521, http://dx.doi.org/10.1121/1.391434.
[4] S.D. Lubetkin, The fundamentals of bubble evolution, Chem. Soc. Rev. 24 (1995) 243–250, http://dx.doi.org/10.1039/CS9952400243.
[5] F.R.S. O.M. Lord Rayleigh VIII, On the pressure developed in a liquid during the collapse of a spherical cavity, Lond. Edinb. Dublin Philos. Mag. J. Sci. 34 (1917) 94–98, http://dx.doi.org/10.1080/14786440808635681.
[6] W.F. Busse, Phys. Rubber As Relat. Automob. J. Appl. Phys. 9 (1938) 438–451, http://dx.doi.org/10.1063/1.1710439.
[7] R.B. Dean, The formation of bubbles, J. Appl. Phys. 15 (1944) 446–451, http://dx.doi.org/10.1063/1.1707453.
[8] J.H. Hollomon, C. Zener, Problems in fracture of metals, J. Appl. Phys. 17 (1946) 82–90, http://dx.doi.org/10.3367/UFNr.0031.194701c.0038.
[9] S. Takagi, Theory of the formation of bubbles, J. Appl. Phys. 24 (1953) 1453–1462, http://dx.doi.org/10.1063/1.1721198.
[10] R.E. Apfel, The role of impurities in cavitation-threshold determination, J. Acoust. Soc. Am. 48 (1970) 1179–1186, http://dx.doi.org/10.1121/1.1912258.

[11] R. Raj, M.F. Ashby, Intergranular fracture at elevated temperature, Acta Metall. 23 (1975) 653–666, http://dx.doi.org/10.1016/0001-6160(75)90047-4.

[12] R.H.S. Winterton, Nucleation of boiling and cavitation, J. Phys. D: Appl. Phys. 10 (1977) 2041–2056, http://dx.doi.org/10.1088/0022-3727/10/15/008.

[13] I.W. Chen, A.S. Argon, Creep cavitation in 304 stainless steel, Acta Metall. 29 (1981) 1321–1333, http://dx.doi.org/10.1016/0001-6160(81)90023-7.

[14] R.E. Apfel, N. Qiu, Principle of dynamic decompression and cooling for materials processing, J. Mater. Res. 11 (1996) 2916–2920, http://dx.doi.org/10.1557/JMR.1996.0369.

[15] T. Kinjo, M. Matsumoto, Cavitation processes and negative pressure, Fluid Phase Equilib. 144 (1998) 343–350, http://dx.doi.org/10.1016/S0378-3812(97)00278-1.

[16] V.M. Fokin, A.S. Abyzov, J.W.P. Schmelzer, E.D. Zanotto, Stress induced pore formation and phase selection in a crystallizing stretched glass, J. Non-Cryst. Solids 356 (2010) 1679–1688, http://dx.doi.org/10.1016/j.jnoncrysol.2010.06.008.

[17] Y. Yang, J. Luo, L. Huang, G. Hu, K.D. Vargheese, Y. Shi, J.C. Mauro, Crack initiation in metallic glasses under nanoindentation, Acta Mater. 115 (2016) 413–422, http://dx.doi.org/10.1016/j.actamat.2016.06.001.

[18] D. Richard, E. Lund, J. Schroers, E. Bouchbinder, Bridging necking and shear-banding mediated tensile failure in glasses, Phys. Rev. Mater. 7 (L032601) (2023) http://dx.doi.org/10.1103/PhysRevMaterials.7.L032601.

[19] J. Banhart, Manufacture, characterisation and application of cellular metals and metal foams, Prog. Mat. Sc. 46 (2001) 559–632, http://dx.doi.org/10.1016/S0079-6425(00)00002-5.

[20] X. Tang, L. Shen, H. Zhang, W. Li, W. Wang, Crack tip cavitation in metallic glasses, J. Non-Cryst. Solids 592 (2022) 121762, http://dx.doi.org/10.1016/j.jnoncrysol.2022.121762.

[21] N. Amigo, Tensile deformation of metallic glass and shape memory alloy nanolaminates, J. Non-Cryst. Solids 635 (2024) 123011, http://dx.doi.org/10.1016/j.jnoncrysol.2024.123011.

[22] B.N. Galimzyanov, A.V. Mokshin, Cavity nucleation in single-component homogeneous amorphous solids under negative pressure, J. Phys.: Condens. Matter. 34 (2022) 414001, http://dx.doi.org/10.1088/1361-648X/ac8462.

[23] A.A. Vakulenko, S.A. Kukushkin, Kinetics of brittle fracture of elastic materials, Phys. the Solid State 40 (1998) 1147–1150, http://dx.doi.org/10.1134/1.1130507.

[24] A.V. Redkov, S.A. Kukushkin, A.V. Osipov, Growth of faceted pores in a multicomponent crystal by applying mechanical stress, CrystEngComm 22 (2020) 5280–5288, http://dx.doi.org/10.1039/D0CE00888E.

[25] P. Guan, S. Lu, M.J.B. Spector, P.K. Valavala, M.L. Falk, Cavitation in amorphous solids, Phys. Rev. Lett. 110 (2013) 185502, http://dx.doi.org/10.1103/PhysRevLett.110.185502.

[26] V. Munizaga, M.L. Falk, The thermodynamic effects of solute on void nucleation in Mg alloys, J. Chem. Phys. 161 (2024) 044509, http://dx.doi.org/10.1063/5.0196513.

[27] V.I. Kalikmanov, Nucleation Theory, in: Lecture Notes in Physics, Springer, New York, 2012.

[28] S. Karthika, T.K. Radhakrishnan, P. Kalaichelvi, A review of classical and nonclassical nucleation theories, Cryst. Growth Des. 16 (2016) 6663–6681, http://dx.doi.org/10.1021/acs.cgd.6b00794.

[29] A.V. Mokshin, B.N. Galimzyanov, Kinetics of crystalline nuclei growth in glassy systems, Phys. Chem. Chem. Phys. 19 (2017) 11340–11353, http://dx.doi.org/10.1039/C7CP00879A.

[30] B.N. Galimzyanov, D.T. Yarullin, A.V. Mokshin, Change in the crystallization features of supercooled liquid metal with an increase in the supercooling level, JETP Lett. 107 (2018) 629–634, http://dx.doi.org/10.1134/S0021364018100089.

[31] V.V. Brazhkin, Can glassforming liquids be simple? Phys.-Usp. 62 (2019) 623–629, http://dx.doi.org/10.3367/UFNe.2018.06.038382.

[32] B.N. Galimzyanov, M.A. Doronina, A.V. Mokshin, Arrhenius crossover temperature of glass-forming liquids predicted by an artificial neural network, Materials 16 (1127) (2023) http://dx.doi.org/10.3390/ma16031127.

[33] B.N. Galimzyanov, M.A. Doronina, A.V. Mokshin, Machine learning-based prediction of elastic properties of amorphous metal alloys, Phys. A 617 (2023) 128678, http://dx.doi.org/10.1016/j.physa.2023.128678.

[34] B.N. Galimzyanov, M.A. Doronina, A.V. Mokshin, Neural network as a tool for design of amorphous metal alloys with desired elastoplastic properties, Metals 13 (812) (2023) http://dx.doi.org/10.3390/met13040812.

[35] B.N. Galimzyanov A.V. Mokshin, Steady-state homogeneous nucleation and growth of water droplets: Extended numerical treatment, J. Phys. Chem. B 116 (2012) 11959–11967, http://dx.doi.org/10.1021/jp304830e.

[36] G.C. Sosso, J. Chen, S.J. Cox, M. Fitzner, P. Pedevilla, A. Zen, A. Michaelides, Crystal nucleation in liquids: Open questions and future challenges in molecular dynamics simulations, Chem. Rev. 116 (2016) 7078–7116, http://dx.doi.org/10.1021/acs.chemrev.5b00744.

[37] V.G. Baidakov, A.O. Tipeev, Molecular dynamics simulation of homogeneous nucleation in a superheated lennard-jones crystal, J. Non-Cryst. Solids 503–504 (2019) 302–307, http://dx.doi.org/10.1016/j.jnoncrysol.2018.10.007.

[38] T. Eggert, N.G. Hørmann, K. Reuter, Cavity formation at metal–water interfaces, J. Chem. Phys. 159 (2023) 194702, http://dx.doi.org/10.1063/5.0167406.

[39] T.S. Chow, Wetting of rough surfaces, J. Phys.: Condens. Matter. 10 (1998) L445–L451, http://dx.doi.org/10.1088/0953-8984/10/27/001.

[40] F. Meixner, M.R. Ahmadi, C. Sommitsch, Cavity nucleation and growth in nickel-based alloys during creep, Materials 15 (1495) (2022) http://dx.doi.org/10.3390/ma15041495.

[41] M.E. Kassner, T.A. Hayes, Creep cavitation in metals, Int. J. Plast. 19 (2003) 1715–1748, http://dx.doi.org/10.1016/S0749-6419(02)00111-0.

[42] D.J. Evans, G.P. Morriss, Statistical Mechanics of Non-Equilibrium Liquids, Cambridge University, New-York, 2008.

[43] A.P. Thompson, S.J. Plimpton, W. Mattson, General formulation of pressure and stress tensor for arbitrary many-body interaction potentials under periodic boundary conditions, J. Chem. Phys. 131 (2009) 154107, http://dx.doi.org/10.1063/1.3245303.

[44] P. Hänggi, P. Talkner, M. Borkovec, Reaction-rate theory: fifty years after kramers, Rev. Modern Phys. 62 (1990) 251–341, http://dx.doi.org/10.1103/RevModPhys.62.251.

[45] A.V. Mokshin, B.N. Galimzyanov, Scaling law for crystal nucleation time in glasses, J. Chem. Phys. 142 (2015) 104502, http://dx.doi.org/10.1063/1.4914172.

[46] Y. Zhang, R. Ashcraft, M.I. Mendelev, C.Z. Wang, K.F. Kelton, Experimental and molecular dynamics simulation study of structure of liquid and amorphous $Ni_{62}nb_{38}$ alloy, J. Chem. Phys. 145 (2016) 204505, http://dx.doi.org/10.1063/1.4968212.

[47] M.I. Mendelev, Y. Sun, F. Zhang, C.Z. Wang, K.M. Ho, Development of a semi-empirical potential suitable for molecular dynamics simulation of vitrification in cu-zr alloys, J. Chem. Phys. 151 (2019) 214502, http://dx.doi.org/10.1063/1.5131500.

[48] M.A. Turchanin, P.G. Agraval, A.R. Abdulov, Thermodynamic assessment of the cu-ti-zr system. II. Cu-zr and ti-zr systems, Powder Met. Met. Ceram. 47 (2008) 428–446, http://dx.doi.org/10.1007/s11106-008-9039-x.

[49] B.N. Galimzyanov, M.A. Doronina, A.V. Mokshin, Unusual effect of high pressures on phase transformations in $Ni_{62}nb_{38}$ alloy, J. Phys. Chem. Solids 171 (2022) 110995, http://dx.doi.org/10.1016/j.jpcs.2022.110995.

[50] A. Stukowski, Computational analysis methods in atomistic modeling of crystals, 66, 2014, pp. 399–407, http://dx.doi.org/10.1007/s11837-013-0827-5.

[51] I.L. Shereshevsky, Surface tension of saturated vapours and the equation of eötvös, J. Phys. Chem. 35 (1931) 1712–1720, http://dx.doi.org/10.1021/j150324a014.

[52] A.K. Dureja, S.K. Sinha, A. Srivastava, R.K. Sinha, J.K. Chakravartty, P. Seshu, D.N. Pawaskar, Flow behaviour of autoclaved, 20% cold worked, Zr-2.5Nb alloy pressure tube material in the temperature range of room temperature to 800 °C, J. Nucl. Mater. 412 (2011) 22–29, http://dx.doi.org/10.1016/j.jnucmat.2011.01.023.

[53] K.-H. Bae, H.-H. Kim, S.-B. Lee, A simple life prediction method for 304L stainless steel structures under fatigue-dominated thermo-mechanical fatigue loadings, Mater. Sci. Eng. A 529 (2011) 370–377, http://dx.doi.org/10.1016/j.msea.2011.09.045.

[54] H. Wang, Y. Hu, X.-Q. Wang, Z. Tao, S.-L. Tang, X.-P. Pang, Y.F. Chen, Behaviour of austenitic stainless steel bolts at elevated temperatures, Eng. Struct 235 (2021) 111973, http://dx.doi.org/10.1016/j.engstruct.2021.111973.

[55] H. Ban, Q. Yang, Y. Shi, Z. Luo, Constitutive model of high-performance bolts at elevated temperatures, Eng. Struct 233 (2021) 111889, http://dx.doi.org/10.1016/j.engstruct.2021.111889.

[56] J. Chen, B. Young, Experimental investigation of cold-formed steel material at elevated temperatures, Thin-Walled Struct. 45 (2007) 96–110, http://dx.doi.org/10.1016/j.tws.2006.11.003.

[57] Y. He, W. Li, M. Yang, Y. Li, X. Zhang, Z. Zhao, P. Dong, J. Ma, S. Zheng, Modeling of temperature-dependent ultimate tensile strength for metallic materials, J. Constr. Steel Res. 191 (2022) 107184, http://dx.doi.org/10.1016/j.jcsr.2022.107184.

[58] M. Asato, T. Hoshino, First-principles calculations for vacancy formation energies in Cu-based alloys, J. Magn. Magn. Mater. 272–276 (2004) 1372–1373, http://dx.doi.org/10.1016/j.jmmm.2003.12.103.

[59] M. Manna, S. Pal, Evaluation of $Ni_{62}Nb_{38}$ bimetallic glass formation under hydrostatically pressurised quenching, Mater. Sci. Forum 978 (2020) 436–445, http://dx.doi.org/10.4028/www.scientific.net/MSF.978.436.

[60] K.P. Tai, L.T. Wang, B.X. Liu, Distinct atomic structures of the Ni-Nb metallic glasses formed by ion beam mixing, J. Appl. Phys. 102 (2007) 124902, http://dx.doi.org/10.1063/1.2825407.

[61] T.D. Xu, X.D. Wang, H. Zhang, Q.P. Cao, D.X. Zhang, J.Z. Jiang, Structural evolution and atomic dynamics in Ni-Nb metallic glasses: A molecular dynamics study, J. Chem. Phys. 147 (2017) 144503, http://dx.doi.org/10.1063/1.4995006.

[62] M.J. Kramer H.W. Sheng, Relating dynamic properties to atomic structure in metallic glasses, JOM 64 (2012) 856–881, http://dx.doi.org/10.1007/s11837-012-0360-y.

[63] V.M. Fokin A.S. Abyzov, Theory of pore formation in glass under tensile stress: Generalized gibbs approach, J. Non-Cryst. Solids 357 (2011) 3474–3479, http://dx.doi.org/10.1016/j.jnoncrysol.2011.06.021.

[64] Q. An, G. Garrett, K. Samwer, Y. Liu, S.V. Zybin, S.-Ni. Luo, M.D. Demetriou, W.L. Johnson, W.A. Goddard, Atomistic characterization of stochastic cavitation of a binary metallic liquid under negative pressure, J. Phys. Chem. Lett. 2 (2011) 1320–1323, http://dx.doi.org/10.1021/jz200351m.

[65] B. Sarac, D. Sopu, E. Park, J.K. Hufenbach, S. Oswald, M. Stoica, J. Eckert, Mechanical and structural investigation of porous bulk metallic glasses, Metals 5 (2015) 920–933, http://dx.doi.org/10.3390/met5020920.

[66] L.-Q. Shen, J.-H. Yu, X.-C. Tang, B.-A. Sun, Y.-H. Liu, H.-Y. Bai1, W.-H. Wang, Observation of cavitation governing fracture in glasses, Sci. Adv. 7 (2021) eabf7293, https://www.science.org/doi/10.1126/sciadv.abf7293.

[67] B. Sarac, B. Klusemann, T. Xiao, S. Bargmann, Materials by design: An experimental and computational investigation on the microanatomy arrangement of porous metallic glasses, Acta Mater. 77 (2014) 411–422.

[68] C.M. Barr, T. Duong, D.C. Bufford, Z. Milne, A. Molkeri, N.M. Heckman, D.P. Adams, A. Srivastava, K. Hattar, M.J. Demkowicz, B.L. Boyce, Autonomous healing of fatigue cracks via cold welding, Nature 620 (2023) 552–556, http://dx.doi.org/10.1038/s41586-023-06223-0.

[69] H. Yu, J. Shao, S. Shuai, C. Chen, L. Wang, D. San-Martín, W. Xu, The application of self-healing concept in Ni superalloys: Theoretical design and experimental validation, Mater. Des. 237 (2024) 112587, http://dx.doi.org/10.1016/j.matdes.2023.112587.

[70] J.V. Jain, V.K. Barnwal, A.K. Saxena, P.B. Nair, K.U. Yazar, S. Suwas, Predicting crack nucleation in commercially pure titanium using orientation imaging microscopy and machine learning, Mater. Lett. 379 (2025) 137593, http://dx.doi.org/10.1016/j.matlet.2024.137593.